Electronic Supplementary Material (ESI) for New Journal of Chemistry.
This journal is © The Royal Society of Chemistry and the Centre National de la Recherche Scientifique 2021

Electronic Supplementary Material (ESI) for CrystEngComm.
This journal is © The Royal Society of Chemistry 2020

Electronic Supporting Information (ESI†)

The $\{PMo_6O_{24}N_4\}$ subunit functionalized by organonitrogen through Mo-N bonds: hydrothermal synthesis, structure, photocatalytic and fluorescence sensing properties

Haiyan Yu, Jun Ying*, Chenxi Sun, Liang Jin, Aixiang Tian, Xiuli Wang*

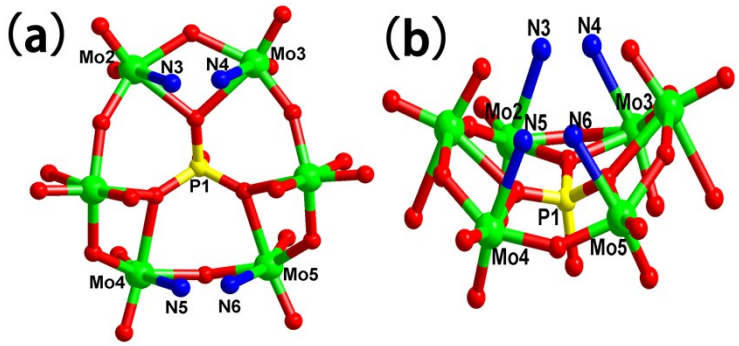

Fig. S1 The unit diagram of the of the $\{PMo_6\}$ polyanion viewing along the front (a) and side (b) respectively.

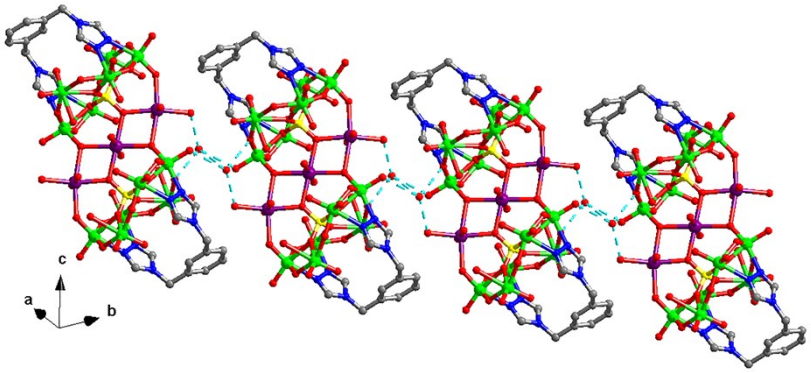

Fig. S2 The 1D supramolecular structure of compound **1** through hydrogen bonding interactions.

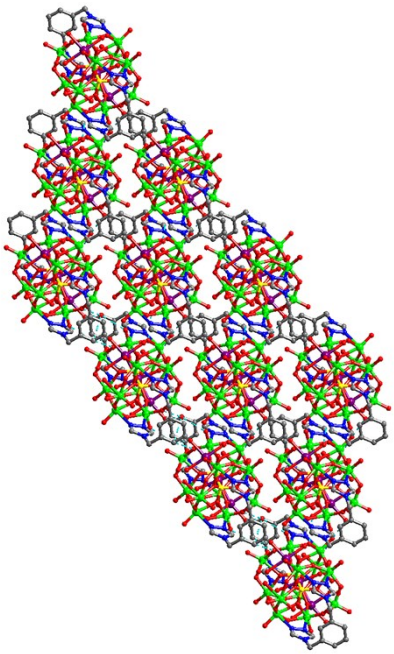

Fig. S3 The 2D supramolecular structure of compound **1**.

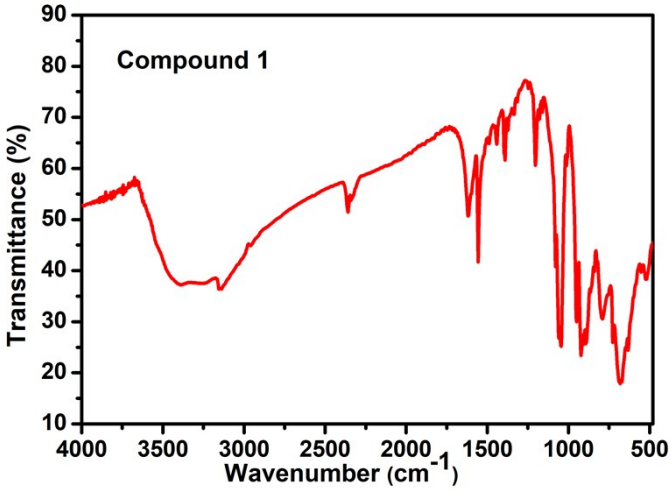

Fig. S4 The IR spectra of compound **1**.

The IR spectra of compound **1** is shown in Fig. S4. The characteristic peaks at 779, 680 and 630 cm^{-1} are attributed to ν(Mo-O_b) vibrations, respectively. The characteristic peaks at 930 and 889 cm^{-1} are attributed to ν(Mo-O_t) vibrations. The characteristic peak of strong absorption band in 1075 cm^{-1} is attributed to the P-O vibration. The peaks in the range of 1630–1392 cm^{-1} could be regarded as the characteristic bands of the organic ligand. The vibration bands around 3350 cm^{-1} are indicative of the presence of lattice water molecules.

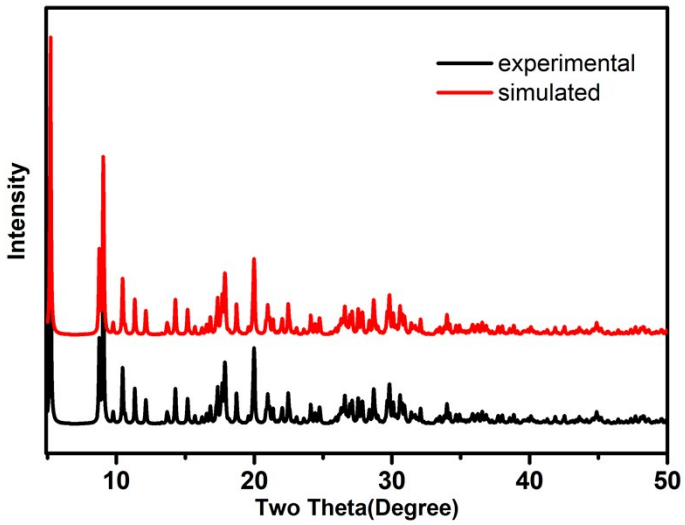

Fig. S5 The PXRD pattern of the compound **1**.

Fig. S5 shows the PXRD pattern of the compound **1**. The experimental results clearly show that the result obtained from the test is consistent with the simulated spectrum, which indicates that the sample has very good phase purity.

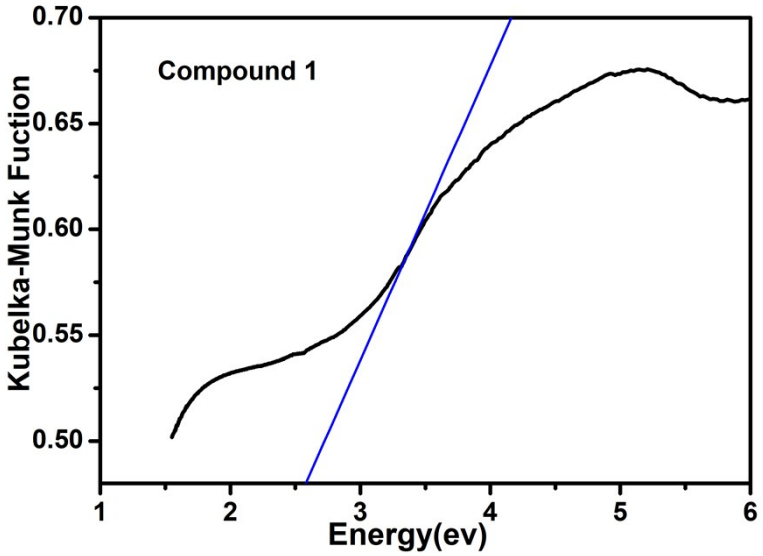

Fig. S6 Kubelka-Munk-transformed diffuse reflectance spectra of compound **1**.

Use a mortar to fully grind the crystal **1** into powder and measure its optical solid-state diffuse reflectance spectrum analysis. The purpose is to obtain the conductivity of the compound and further obtain its band gap value (Eg). The energy band gap (Eg) obtained by extrapolating the linear part of the absorption edge is approximately 2.57 eV (see Fig. S6), indicating its semiconductor property. It further proves that it has an applicable photocatalytic ability.

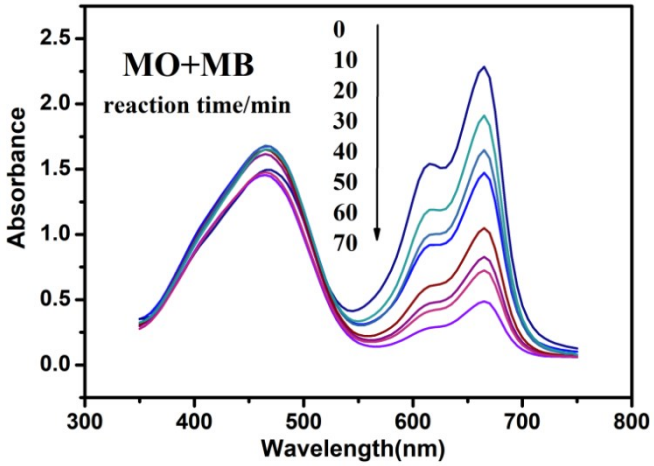

Fig. S7 **Absorption spectra of the MO-MB solution during the decomposition reaction under UV irradiation with the presence of compound.**

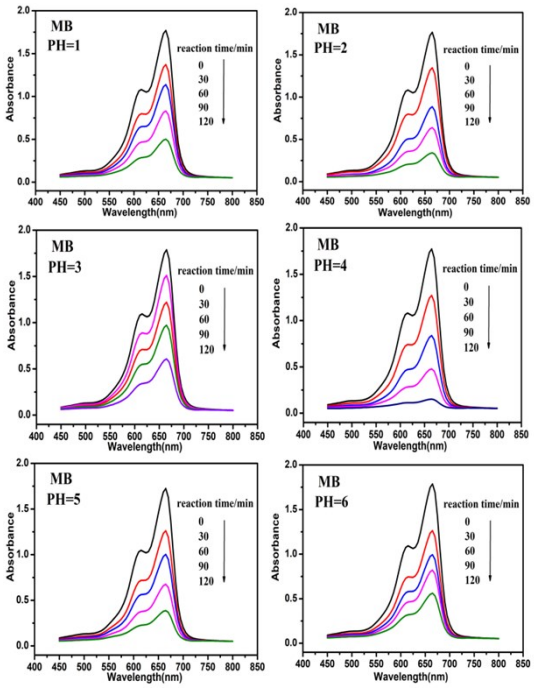

1.

Fig. S8 Photocatalytic degradation of MB under different pH conditions within 120 minutes.

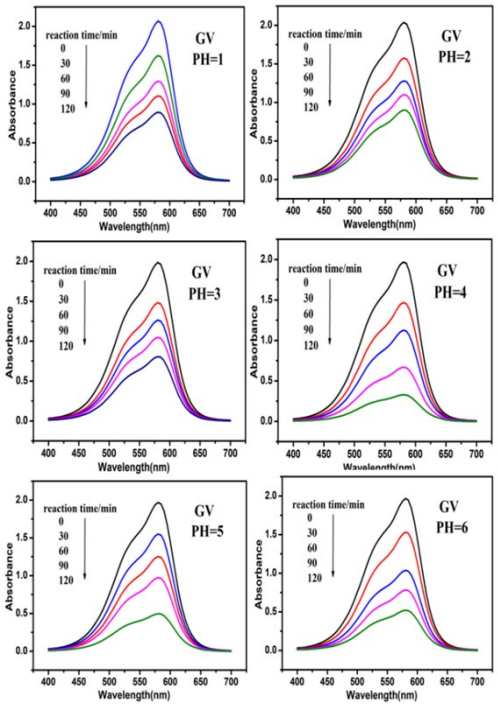

Fig. S9 Photocatalytic degradation of GV under different pH conditions within 120 minutes.

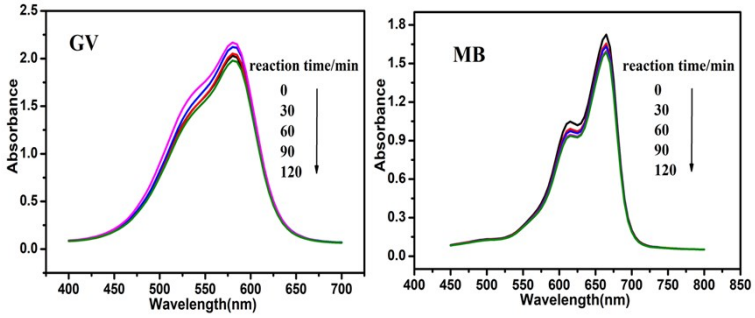

Fig. S10 Without adding catalyst **1**, the absorbance values of GV (left) and MB (right) change within 120 minutes.

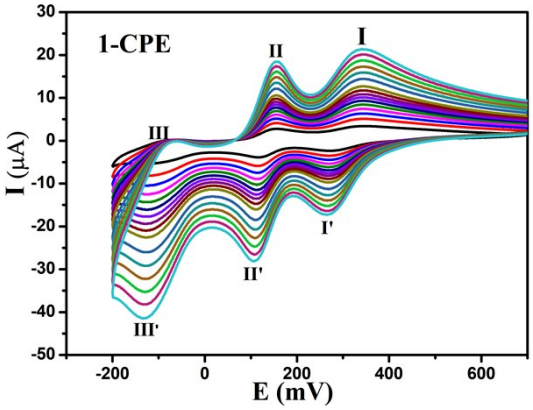

Fig. S11 The cyclic voltammograms of **1**–CPE in 30 ml mixed 0.1 M H_2SO_4 + 0.5 M Na_2SO_4 aqueous solution at different scan rates (from inner to outer: 20, 40, 60, 80, 100, 120, 140, 160, 180, 200, 250, 300, 350, 400, 450 and 500 $mV \cdot s^{-1}$).

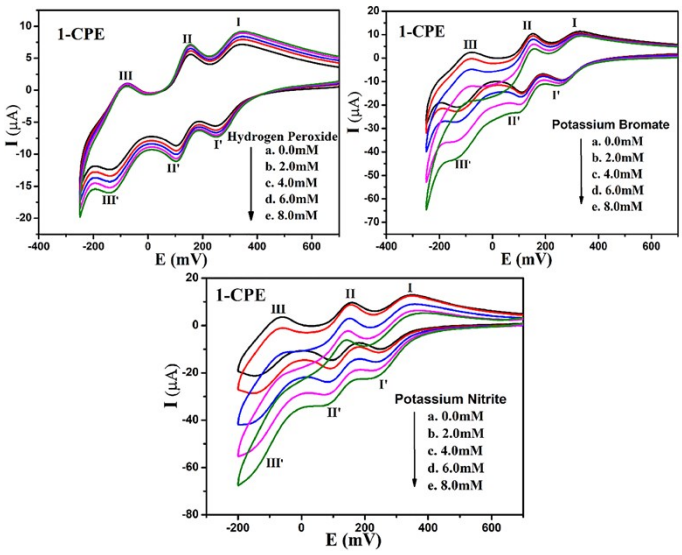

Fig. S12 Cyclic voltammograms of the **1**–CPE in 0.1 M H_2SO_4 + 0.5 M Na_2SO_4 aqueous solution containing 0 (a); 2 (b); 4 (c); 6 (d) and 8 (e) mM H_2O_2, BrO_3^-, NO_2^- and AA. Scan rate: 250 $mV \cdot s^{-1}$.

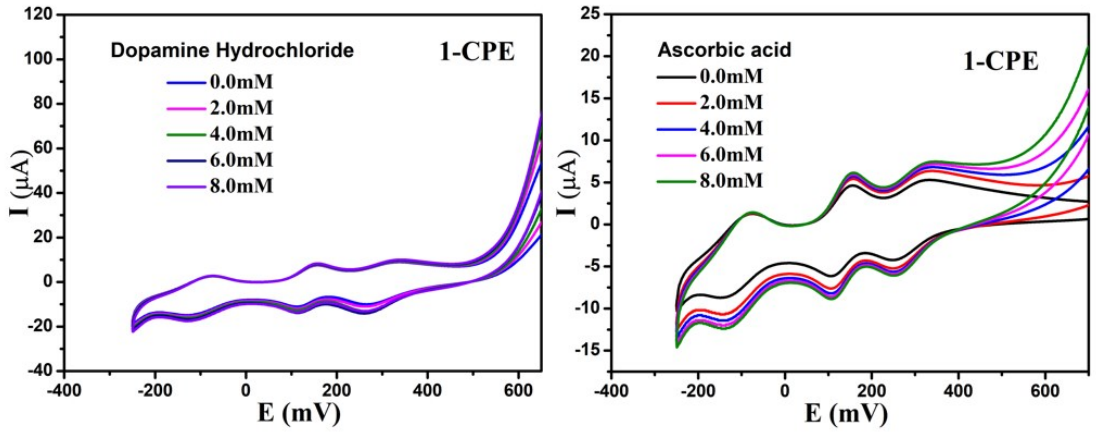

Fig. S13 The usage of **1**–CPE to catalyze the oxidation of dopamine hydrochloride (DP) and ascorbic acid (AA) (scan rate: 250 $mV \cdot s^{-1}$)

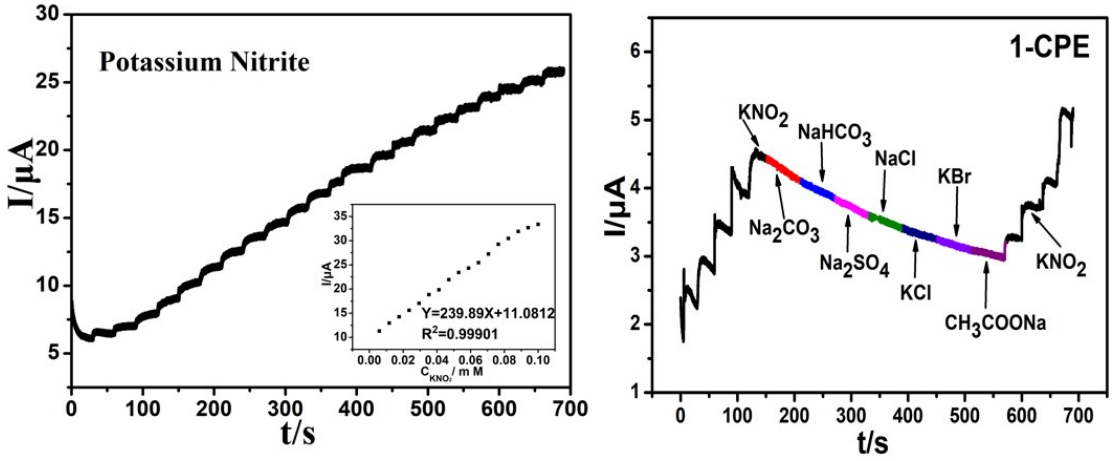

Fig. S14 Left: Amperometric response for the **1**–CPE on successive addition of 0.1 mM nitrite to 0.1 M H_2SO_4+0.5 M Na_2SO_4 aqueous solution. The inset: the steady-state calibration curve for current versus hydrogen peroxide concentration. Right: Amperometric current responses of **1**–CPE in aqueous solution upon addition of various inorganic salts.

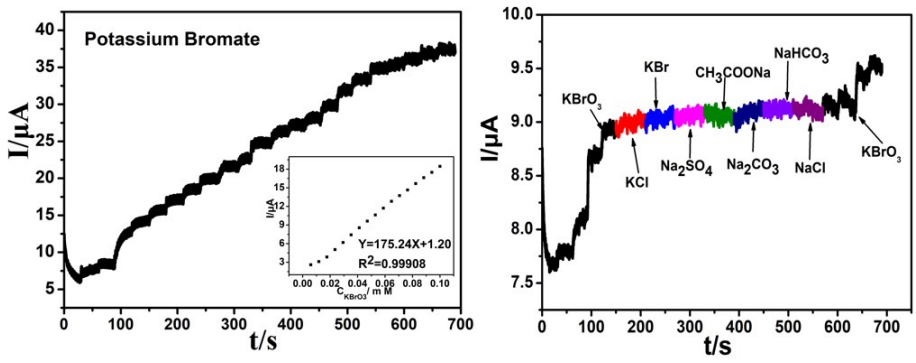

Fig. S15 Left: Amperometric response for the **1**–CPE on successive addition of 0.1 mM bromate to 0.1 M H_2SO_4+0.5 M Na_2SO_4 aqueous solution. The inset: the steady-state calibration curve for current versus hydrogen peroxide concentration. Right: Amperometric current responses of **1**–CPE in aqueous solution upon addition of various inorganic salts.

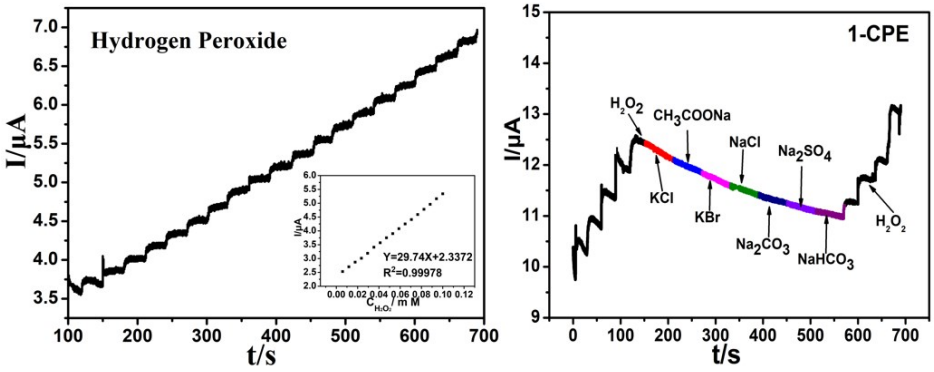

Fig. S16 Left: Amperometric response for the **1**–CPE on successive addition of 0.1 mM hydrogen peroxide to 0.1 M H_2SO_4+0.5 M Na_2SO_4 aqueous solution. The inset: the steady-state calibration curve for current versus hydrogen peroxide concentration. (b) Amperometric current responses of **1**–CPE in aqueous solution upon addition of various inorganic salts.

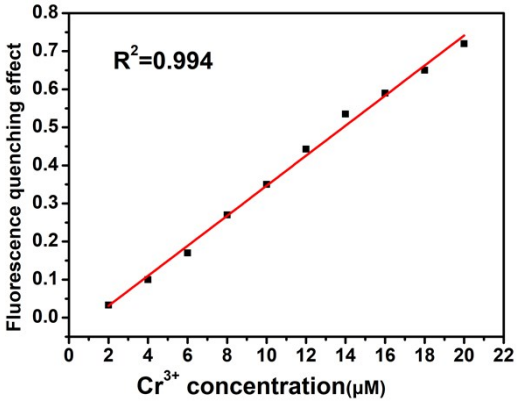

Fig. S17 The linear relationship of the fluorescence quenching effect with increasing of Cr^{3+} concentration.

Table. S1. Crystal Data and Structure Refinement Parameters for Compound **1**.

formula	$C_{24}\ H_{50}\ Cd_3\ Mo_{12}\ N_{12}\ O_{57}\ P_2$
fw	2963
cryst syst	Triclinic
space group	P -1
a (Å)	10.2923(18)
b (Å)	10.3806(18)
c (Å)	17.587(3)
V(Å^3)	1763.8(5)
Z	1
D_c (g cm^{-3})	2.805
R_{int}	0.0269
GOF	1.041
R_1[a][I>2sigma(I)]	0.0543
wR_2[b] (all data)	0.1642

[a]$R_1 = \Sigma||F_o|-|F_c||/\Sigma|F_o|$; [b]$wR_2 = \Sigma[w(F_o^2-F_c^2)^2]/\Sigma[w(F_o^2)^2]^{1/2}$

Table. S2. Selected bond distances (Å) and angles (°) for compound **1**.

Cd(1)-O(18)#1	2.265(5)	Cd(2)-O(3)	2.205(7)
Cd(1)-O(19)	2.298(6)	Cd(2)-O(2)	2.268(7)
Cd(1)-O(9)	2.331(6)	Cd(2)-O(9)#1	2.445(6)
Cd(2)-O(18)	2.245(5)	Cd(2)-O(1)	2.241(7)
Cd(2)-O(4)	2.330(6)	N(6)-N(5)-Mo(4)	119.2(5)
O(18)#1-Cd(1)-O(18)	180.0	O(18)-Cd(1)-O(19)	83.5(2)
O(18)#1-Cd(1)-O(19)	96.5(2)	O(1)-Cd(2)-O(2)	81.5(3)
O(18)-Cd(1)-O(9)#1	78.55(19)	O(4)-Cd(2)-O(9)#1	168.0(2)
O(18)-Cd(1)-O(9)	101.45(19)	O(3)-Cd(2)-O(18)	96.6(3)
O(19)-Cd(1)-O(19)#1	180	O(3)-Cd(2)-O(1)	97.6(3)
O(19)-Cd(1)-O(9)#1	90.6(2)	O(3)-Cd(2)-O(4)	95.1(3)
O(19)-Cd(1)-O(9)	89.4(2)	O(3)-Cd(2)-O(9)#1	82.9(3)

O(9)-Cd(1)-O(9)#1	180	O(3)-Cd(2)-O(2)	174.9(3)
O(18)-Cd(2)-O(4)	92.0(2)	O(2)-Cd(2)-O(4)	90.0(3)
O(18)-Cd(2)-O(9)#1	76.56(19)	O(2)-Cd(2)-O(9)#1	92.2(3)
O(18)-Cd(2)-O(2)	83.4(2)	O(24)-Mo(5)-N(6)	79.4(3)
O(1)-Cd(2)-O(18)	163.1(2)	O(25)-Mo(5)-N(6)	91.4(3)
O(1)-Cd(2)-O(4)	95.7(2)	O(26)-Mo(5)-N(6)	75.6(3)
O(1)-Cd(2)-O(9)#1	96.3(2)	O(1)-Cd(2)-O(2)	81.5(3)
O(4)-Cd(2)-O(9)#1	168.0(2)	O(7)-Mo(2)-N(3)	90.9(3)
O(3)-Cd(2)-O(18)	96.6(3)	O(9)-Mo(2)-N(3)	164.8(3)
O(3)-Cd(2)-O(1)	97.6(3)	O(6)-Mo(3)-N(4)	92.9(3)
O(3)-Cd(2)-O(4)	95.1(3)	O(11)-Mo(3)-N(4)	72.3(2)
O(3)-Cd(2)-O(9)#1	82.9(3)	O(10)-Mo(3)-N(4)	78.0(3)
O(3)-Cd(2)-O(2)	174.9(3)	O(8)-Mo(3)-N(4)	75.4(3)
O(2)-Cd(2)-O(4)	90.0(3)	O(5)-Mo(3)-N(4)	161.7(3)
O(2)-Cd(2)-O(9)#1	92.2(3)	Cd(2)-O(18)-Cd(1)	106.3(2)
O(24)-Mo(5)-N(6)	79.4(3)	P(1)-O(18)-Cd(1)	120.9(3)
O(25)-Mo(5)-N(6)	91.4(3)	P(1)-O(18)-Cd(2)	132.9(3)
O(26)-Mo(5)-N(6)	75.6(3)	Cd(2)-O(1)-H(1A)	126.2
O(23)-Mo(5)-N(6)	80.1(2)	Cd(2)-O(1)-H(1B)	125.8
O(4)-Mo(5)-N(6)	163.5(3)	Cd(1)-O(19)-H(19A)	111.8
O(27)-Mo(4)-N(5)	87.5(3)	Cd(1)-O(19)-H(19B)	111.7
O(26)-Mo(4)-N(5)	75.1(3)	Mo(5)-O(4)-Cd(2)	131.5(3)
O(21)-Mo(4)-N(5)	81.8(2)	Cd(1)-O(9)-Cd(2)#1	98.1(2)
O(20)-Mo(4)-N(5)	80.3(3)	Mo(2)-O(9)-Cd(1)	130.2(3)
O(22)-Mo(4)-N(5)	167.4(3)	Mo(2)-O(9)-Cd(2)#1	129.5(3)
O(12)-Mo(2)-N(3)	78.9(3)	C(1)-N(4)-Mo(3)	134.3(7)
O(11)-Mo(2)-N(3)	71.8(2)	N(5)-N(6)-Mo(5)	118.4(5)
O(8)-Mo(2)-N(3)	75.6(2)	C(12)-N(6)-Mo(5)	134.5(6)
O(4)-Cd(2)-O(9)#1	168.0(2)	O(7)-Mo(2)-N(3)	90.9(3)

N(4)-N(3)-Mo(2)	115.2(5)	C(11)-N(5)-Mo(4)	132.9(6)
C(2)-N(3)-Mo(2)	137.3(6)	C(11)-N(5)-N(6)	107.6(7)
C(2)-N(3)-N(4)	106.4(7)	Cd(2)-O(3)-H(3A)	113.1
C(2)-N(2)-C(3)	125.3(9)	Cd(2)-O(3)-H(3B)	138.5
C(1)-N(2)-C(2)	106.0(7)	Cd(2)-O(2)-H(2A)	119.2
C(1)-N(2)-C(3)	128.7(8)	Cd(2)-O(2)-H(2B)	135.8

Symmetry codes:#1 -x+1,-y+1,-z+1

Table S3. The analytical data for **1**–CPE as amperometric sensors.

substances	Temperature	Response time	Concentration range	Sensitivity	Correlation coefficient	Detection limit
H_2O_2	25	2.7s	4×10^{-3}–9.2×10^{-2} mM	28.69 μA mM^{-1}	0.99989	1.1×10^{-5} M
$KBrO_3$	25	3.2s	4×10^{-3}–9.2×10^{-2} mM	169.33 μA mM^{-1}	0.99942	6.8×10^{-4} M
KNO_2	25	2.4s	4×10^{-3}–9.2×10^{-2} mM	239.89 μA mM^{-1}	0.99901	4.2×10^{-4} M